Thermalization and prethermalization in the soft-wall AdS/QCD model

Xuanmin Cao,[1] Jingyi Chao,[2,*] Hui Liu,[1] and Danning Li[1,†]

[1]*Department of Physics and Siyuan Laboratory, Jinan University, Guangzhou 510632, China*
[2]*College of Physics and Communication Electronics, Jiangxi Normal University, Nanchang, Jiangxi 330022, China*

(Received 22 October 2022; accepted 16 March 2023; published 3 April 2023)

The real-time dynamics of chiral phase transition is investigated in a two-flavor ($N_f = 2$) soft-wall anti–de Sitter/QCD model. To understand the dynamics of thermalization, we quench the system from initial states deviating from the equilibrium states. Then, we solve the nonequilibrium evolution of the order parameter (chiral condensate $\langle \sigma \equiv \bar{q}q \rangle$). It is shown that the system undergoes an exponential relaxation at temperatures away from the critical temperature T_c. The relaxation time diverges at T_c, presenting a typical behavior of critical slowing-down. Numerically, we extract the dynamic critical exponent z and get $z \approx 2$ by fitting the scaling behavior $\sigma \propto t^{-\beta/(\nu z)}$, where the mean-field static critical exponents (order parameter critical exponent $\beta = 1/2$, correlation length critical exponent $\nu = 1/2$) have been applied. More interestingly, it is remarked that, for a large class of initial states, the system would linger over a quasi-steady-state for a certain period of time before the thermalization. It is suggested that the interesting phenomenon, known as prethermalization, has been observed in the framework of holographic models. In such prethermal stage, we verify that the system is characterized by a universal dynamical scaling law and described by the initial-slip exponent $\theta = 0$.

DOI: 10.1103/PhysRevD.107.086001

I. INTRODUCTION

The nonequilibrium dynamics plays an essential role from the high-energy physics and cosmology to condensed matter physics, at which relevant physical properties exhibit universal dynamic scaling behavior. The observed phenomena in relativistic heavy-ion collisions [1] lead to a consistent framework of bulk QCD matter evolutions and critical fluctuations, which has become significantly important to address the critical slowing-down near a critical point [2] and to reveal the domain formation at the first-order phase transition [3]. Recently, the precision cosmology has firmly supported the big bang paradigm [4]. The description of the cosmological fluctuations and the subsequent dynamical response are, in particular, required to establish the scenarios of the baryon asymmetry and the dark matter production [5]. In quantum systems of ultracold atomic gases [6], eventually, many out-of-equilibrium progresses are set into the context of universal dynamics in recent decades [7].

Among very different physical systems, a universal time evolution appearing in the early-time regime was discovered by Berges *et al.* in Ref. [8] through a quark-meson model. It is found that, governed by the strong fields or large occupancy of modes, a transient occurs in the far-from-equilibrium initial conditions, named as prethermalization. The observed evolution suggests that the systems are usually passing in the vicinity of a nonthermal fixed point (NTFP) before approaching the long time thermalization [8,9]. In regard to the numerical value of the scaling exponents, one observes that several macroscopic properties of the underlying system play a vital role, such as the number of spatial dimensions and whether the particle or energy cascade is being produced. Many relevant works of prethermalization have been completed within a variety of many-body models after sudden quenches of the phase transition parameters. In general, they can be classified into isolated systems [10–15] and open systems [16,17]. In a few integrable isolated systems, the prethermal states turn out to be described by the generalized Gibbs ensemble [18–20], though a general conclusion for any system is not reached yet. Under the renormalization group flow frame, the behaviors near the NTFP have been discussed [13–15].

On the other hand, prior to reaching equilibrium, another possible preequilibrium critical phenomena emerges as the memory of the initial condition during the early stage and

*Corresponding author.
chaojingyi@jxnu.edu.cn
†Corresponding author.
lidanning@jnu.edu.cn

instead has been discovered earlier by Janssen *et al.* [21]. In the regime near the continuous phase transition, the initial preparation extends to all times in a manner similar to the surface critical phenomena. To describe the distribution width of initial configurations, the universal initial-slip exponent θ is proposed in the pioneering work of [21] with a pure dissipative classical system. Here, the universal collective behavior is developed in the time window between the microscopic timescales and the translationally invariant asymptotics. Critical exponent θ specifically characterizes the breaking of the time translation invariance due to the initial conditions. The study of short time scaling has already attracted much attention in the toy model of ϕ^4 theory through the nonequilibrium renormalization group method [21–23] and by the large N expansion [24]. In many other open systems, further investigations on the short time dynamical scaling are currently under active exploration [25].

While the unusual initial states are created in the off-central heavy-ion collisions, we expect that a potentially unique signature of magnetic fields would be manifested in the out-of-equilibrium evolution near the critical end point. Generally, an ultrastrong magnetic field is produced by the fast colliding, highly charged nuclei in heavy-ion experiments, and the strength of the eB field is at the order of m_π^2 [26]. However, the duration of the magnetic field remains an open question. A reasonable estimation is that the lifetime of the eB field is as long as the starting time of the hydrodynamic evolution, ~0.6 fm [27]. The rapidly decayed magnetic field leads to an undetectable signal of the chiral magnetic effect [28]. As it turned out, such a quickly disappeared field could serve as a randomly prepared initial state for the evolution of the hydrodynamic quark-gluon plasma. And we expect that the short time scaling is nevertheless encoded in the evolutions of two- and higher-point correlation functions [29]. The influence of the initial-slip exponent in the context of heavy-ion collisions is not yet completed, in contrast with the relativistic hydrodynamics [30]. This is because a full theory that incorporates the fluctuations near the phase transition and bulk evolution in strongly coupling plasma is currently under construction.

As a powerful tool for addressing strongly coupled gauge theories, the holographic duality has successfully predicted a lower bound of the shear viscosity over the volume density of entropy $\eta/S \leq 1/4\pi$ [31–33]. Impressively, the holographic method not only takes advantage of addressing the near equilibrium phenomena for strongly coupling systems in a perturbative manner, but it is also adept at studying the far-from-equilibrium dynamic processes. For the out-of-equilibrium dynamics, it is proposed that the linear relaxation is corresponding to the quasinormal mode (QNM) of the black hole in the AdS/CFT correspondence [34]. The nonequilibrium dynamics in the holographic model actually is the problem in classical general relativity, which can be solved with numerical relativity. The holographic duality has been successfully used to study the far-from-equilibrium dynamic phenomena, for example, the Kibble-Zurek mechanics in the holographic superfluid or superconductivity [35–38], the NTFP in the holographic superfluid [39], and the holographic thermalization of super Yang-mills theory and QCD [40–46].

In this work, we will study the nonequilibrium physics of QCD matter in the holographic framework, focusing on both the long time thermalization and the short time scaling behavior. Therefore, a holographic description of both the light modes and phase transitions would be quite necessary. In the bottom-up approach, the soft-wall anti–de Sitter (AdS)/QCD model proposed in Ref. [47] does provide an effective scenario to consider the light meson spectrum [48–61] and chiral phase transition [62–71], as well as the pion condensed phase [72,73]. Thus, we will take the soft-wall model as our starting point.

The paper is organized as follows. We will introduce the soft-wall AdS/QCD model and holographic chiral phase transition in Sec. II. Then, in Sec. III, we will verify the linear relaxation and the critical slowing-down with the time-dependent sigma condensate in the soft-wall AdS/QCD model, as well as the relations between the thermalization and the QNM. In Sec. IV, we will study the prethermalization, as well as the crossover to the thermalization through different quench protocols. The short time dynamic exponent is numerically fitted and $\theta = 0$. Finally, conclusions and discussion are given in Sec. V.

II. THE SOFT-WALL AdS/QCD MODEL AND CHIRAL PHASE TRANSITION

In this section, we will briefly review the soft-wall AdS/QCD model, which is a bottom-up holographic QCD model, based on the global $\mathrm{SU}(N_f)_L \times \mathrm{SU}(N_f)_R$ chiral flavor symmetry. The original soft-wall model was proposed by Karch *et al.* in Ref. [47]. As mentioned above, by slightly extending the original soft-wall model, the chiral phase transition and light meson spectra could be well described. Furthermore, the mass diagram of chiral phase transition could be realized [74], in which a critical point appears in the two-flavor chiral limit. Thus, it provides an ideal starting point for the main interests of this work.

In the soft-wall models, the background metric is usually taken as the AdS metric

$$ds^2 = e^{2A(r)}(-dr^2 + \eta_{\mu\nu}dx^\mu dx^\nu), \tag{1}$$

where $A(r) = -\ln r$, $\eta_{\mu\nu} = \mathrm{diag}(1,-1,-1,-1)$, x^μ represents the 4D time and space dimensions, and r represents the fifth dimension. In this work, we concentrate on the bulk scalar field part and neglect the gauge field part of the 5D action. Thus, the 5D action in the bulk is

$$S = \int d^5x e^{-\Phi(r)}\sqrt{g}\mathrm{Tr}\{|DX|^2 - (m_5^2|X|^2 + \lambda|X|^4)\}, \tag{2}$$

in which X is the bifundamental scalar field, m_5 is the 5D mass of X, $\sqrt{g}$ is the determinant of the metric, and λ is a fitting parameter of the quartic term of the potential. $\Phi(r)$ is the dilaton field that is introduced as a smooth cutoff, and it is very essential for the Regge-like behavior of the mass spectrum. For simplicity, we employ the degenerate $N_f = 2$ case with $m_u = m_d = m_q$; thus X can be defined as

$$X = \begin{bmatrix} \frac{\chi+S}{2} & 0 \\ 0 & \frac{\chi+S}{2} \end{bmatrix} \mathrm{Exp}[2i\pi^i t^i], \tag{3}$$

where t^i are the generators of SU(2), S is the scalar perturbation, and π^i are the pseudoscalar perturbations. The near boundary ($r = 0$) expansion of the bulk scalar field $\chi(r)$ could be derived from the equation of motion as

$$\chi(r \to 0) = m_q \gamma r + \cdots + \frac{\sigma}{\gamma} r^3 + \cdots, \tag{4}$$

with the chiral condensate $\sigma = \langle \bar{q} q \rangle$. The parameter $\gamma = \sqrt{N_c}/2\pi$ (the number of colors $N_c = 3$) is a normalization constant, which is fixed by matching the 4D two-point correlator [75].

In thermal medium, one often takes the AdS-Schwarzchild black hole solution as the background metric

$$ds^2 = e^{2A(r)} \left\{ -\frac{1}{f(r)} dr^2 + f(r) dt^2 - d\vec{x}^2 \right\}, \tag{5a}$$

$$f(r) = 1 - \frac{r^4}{r_h^4}, \tag{5b}$$

with the position of the horizon at $r = r_h$ and $0 \le r \le r_h$. From the holographic dictionary, one can identify the temperature T with the Hawking temperature of the black hole

$$T = \frac{1}{\pi r_h}. \tag{6}$$

As shown in Refs. [63,74], the original soft-wall model gives a vacuum without chiral condensate in the chiral limit $m_q = 0$. Therefore, to reproduce the correct behavior, following Ref. [70], we introduce an r-dependent form of the 5D mass m_5^2 and keep the quadratic dilaton, i.e., taking

$$m_5^2 = -3 - \mu_c^2 r^2, \tag{7a}$$

$$\Phi(r) = \mu_g^2 r^2, \tag{7b}$$

where μ_c, μ_g are two model parameters. There could be several possible kinds of origins of this modification. One might consider it as coming from the anomalous dimension correction to the operator dimension $\Delta(r)$, the r (or energy scale) dependence of which would lead to an r dependent $m_5^2(r)$. It could also come from a coupling between X and Φ, representing the interaction of the flavor part with the background, and the mass term would effectively become $m_5^2 \to m_5^2 + h(\Phi)$ with h a function of Φ. As a phenomenological model, here we would not try to derive the exact form of the corrections. Instead, we will mainly focus on the qualitative behavior. So we just follow Ref. [70] and take the simple form in Eq. (7). From our numerical calculation, though the quantitative quantities (like the location of the critical point) would depend on the value of μ_c, the qualitative behavior discussed in this work would not be changed when we change the value of μ_c, guaranteeing the existence of the critical point. Actually, when we take another form of m_5^2 [like $m_5^2 = -3 + \kappa_1 \tanh(\kappa_2 \Phi)$, in another work currently in progress by some of the authors [76]], or even when we take another form of the dilaton field as in Ref. [63], the qualitative results remain the same. Thus, the qualitative behavior discussed below would depend only on the existence of the critical point, and we will stick to the model in Eq. (7) in this work. The values of $\mu_c, \mu_g, m_q, \lambda$ are fitted by the hadron spectra. With $\mu_c = 1450$ MeV, $\mu_g = 440$ MeV, $m_q = 3.22$ MeV, and $\lambda = 80$, it gives a physical pion mass $m_\pi = 139.7$ MeV.

In this model, for any finite quark mass, the chiral phase transition is a crossover. To study the critical phenomena, one has to take the chiral limit $m_q = 0$. In this limit, the crossover transition turns to a second-order transition. After fitting the model parameter by the hadronic spectra, we can study the chiral phase transition in the chiral limit and obtain the critical temperature $T_c \approx 0.16332301$ GeV and the saturation value of the sigma condensate $\sigma_{\mathrm{sat}} \approx 0.015\ \mathrm{GeV}^3$ [56]. It is interesting to see that it is comparable with the results of the critical temperature from lattice QCD and holographic models, like lattice results $T_c = 171 \pm 4$ MeV in Ref. [77] and $T_c = 154 \pm 9$ MeV in Ref. [78], and holographic model results $T_c = 210$ MeV in Ref. [62] and $T_c = 151$ MeV in Ref. [63].

In this work, we will study the universal properties of the nonequilibrium QCD in this IR-modified soft-wall AdS/QCD model. In the soft-wall AdS/QCD model, the mesons are considered as the perturbations on the fixed background metric. In other words, we will consider a subsystem that is coupled to an infinite large heating bath.

III. THERMALIZATION

In the previous studies, the scalar field X is considered as a time-independent field to describe the thermal equilibrium state. To extend those studies to nonequilibrium cases, one has to study the time evolution of X. To avoid the

divergence near the horizon, one would transform the coordinates to the Eddington-Finkelstein (EF) coordinates,

$$t \to v = t - h(r), \tag{8}$$

$$h'(r) = \frac{1}{f(r)}, \tag{9}$$

with a new "time" coordinate v. By properly choosing the integral constant in Eq. (9), one can set $t = v$ at the boundary $r = 0$. Thus, the AdS-Schwarzchild metric becomes

$$ds^2 = e^{2A(r)}\{f(r)dv^2 + 2dvdr - d\vec{x}^2\}. \tag{10}$$

Under the EF coordinate background metric, one obtains the equation of motion (EOM) of χ as[1]

$$\begin{aligned} &2\partial_v\partial_r\chi(v,r) - \left[\frac{3}{r} + \Phi'(r)\right]\partial_v\chi(v,r) - f(r)\partial_r^2\chi(v,r) \\ &+ \left[\frac{3}{r}f(r) + \Phi'(r)f(r) - f'(r)\right]\partial_r\chi(v,r) \\ &+ \frac{1}{r^2}\left(m_5^2 + \frac{\lambda}{2}\chi(v,r)^2\right)\chi(v,r) = 0. \end{aligned} \tag{11}$$

As shown in Refs. [55,74], in the case of $N_f = 2$, the second-order phase transition point (critical point) appears only in the chiral limit. Therefore, we will focus on the two-flavor case with zero quark mass for studying the phenomena in the critical region.

A. Relaxation and critical slowing-down

The static chiral phase transition is a second-order phase transition in the chiral limit, with the symmetry spontaneously breaking from $\mathrm{SU}(2)_L \times \mathrm{SU}(2)_R$ to $\mathrm{SU}_V(2)$. From a previous work, in Ref. [74], the chiral phase transition in the soft-wall model is very similar to the mean-field 3D Ising model, with critical exponents including the order parameter critical exponent $\beta = 1/2$, the correlation length critical exponent $\nu = 1/2$, and the critical exponent of extra-field versus order parameter $\delta = 3$. To extend to nonequilibrium physics, we study the dynamic relaxation properties and the critical slowing-down behavior described by this modified soft-wall AdS/QCD model in this section.

1. Relaxation time

Within the linear response theory [81], either the perturbation taking place in the condensed phase (ordered phase) or in the chiral symmetry restored phase (disordered phase), the sigma condensate $\sigma(t)$ relaxes as

$$\frac{\partial}{\partial t}\sigma(\epsilon,t) = -\frac{\sigma(\epsilon,t) - \sigma_{eq}}{\tau_R}, \tag{12}$$

with the distance to the critical point $\epsilon = (T - T_c)$, the equilibrium sigma condensate $\sigma_{eq} = \sigma(\epsilon,\infty)$, and the relaxation time τ_R. Then, one has $\sigma(\epsilon,t)$,

$$\sigma(\epsilon,t) = \sigma_{eq} + [\sigma(\epsilon,t_0) - \sigma_{eq}]e^{-(t-t_0)/\tau_R}, \tag{13}$$

with the initial sigma condensate $\sigma(\epsilon,t_0)$ at t_0.

Generally, to realize the relaxation process described in Eq. (12), the initial state should slightly deviate from the equilibrium state. We choose a temperature higher than the critical temperature as a final temperature, $T_f = 164\,\mathrm{MeV}$.[2] Generally, the relaxation time τ_R should not depend on the details of the initial state or the way by which the initial state is prepared. The only physical constraint is that the sigma condensate of the initial state should be less than the saturation sigma condensate σ_{sat}. Here, we will try to verify this numerically. We give three different initial states as examples: one has a tiny quark mass, $m_i = 0.1$ MeV; the other one has a temperature slightly below the critical temperature, $T_i = 160$ MeV; and the last one is given a small quantity of sigma condensate, $\sigma_i = 10^{-3}$ GeV^3. We numerically calculate the $\chi(\epsilon,t)$ through Eq. (11) with these three different initial states. As presented in Fig. 1(a), after a microscopic timescale $[\sim 2/(\pi T_f)]$, the system crosses over to the linear relaxation regime, in which sigma condensates behave as exponential decay (linearly decreasing in the semilog plot). Then we choose the initial time of the relaxation at $t_0 = 200\ \mathrm{GeV}^{-1}$ and rescale the time dependence $\sigma(t)$ as shown in Fig. 1(b). The numerical data are well fitted with Eq. (13) which give relaxation times $\tau_R = 111.207$, 111.186, and 111.202 GeV^{-1}, respectively. Within allowable errors, these three different relaxation processes share the same relaxation time, which is determined by the same final state.

When the final state is too far from the critical temperature, the relaxation process behaves differently. For example, we set the system initially at a equilibrium state with $T_i = 110$ MeV, then sudden quench to the final temperature $T_f = 120$ MeV. The evolution curves of the sigma condensate are shown in Fig. 2. Instead of pure relaxation, the evolution of $\sigma(t)$ moves in an oscillation damping mode. However, the damping rate of the sigma condensate is determined by the relaxation time. We fitted the envelope curve with Eq. (13) and got $\tau_R = 10.342\ \mathrm{GeV}^{-1}$, as shown in Fig. 2(b).

[1]We solve the EOM [Eq. (11)] through the pseudospectral method [79,80]. A brief introduction to the solving processes is given in the Appendix.

[2]This temperature ensures that the final equilibrium sigma condensate $\sigma_{\mathrm{eq}} = 0$.

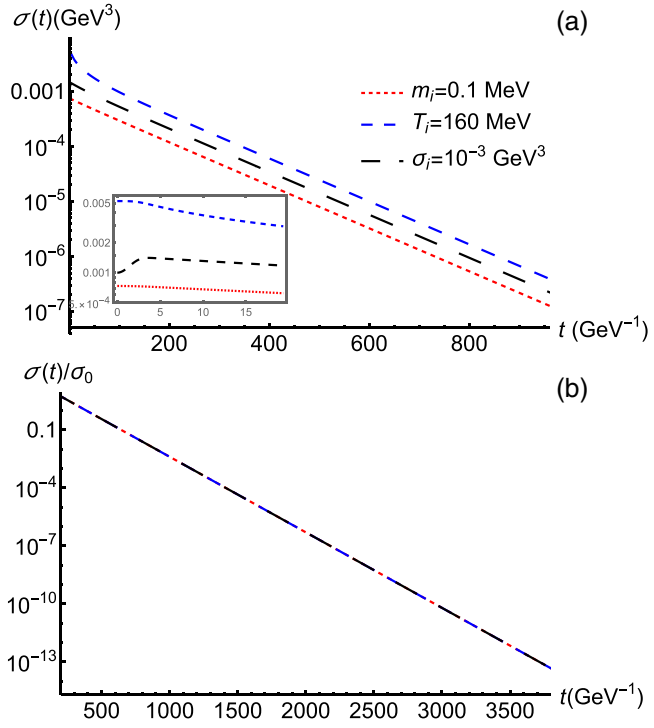

FIG. 1. Relaxation of the sigma condensate $\sigma(t)$ with different initial conditions and final temperature $T_f = 164$ MeV. (a) Time dependence of sigma condensate $\sigma(t)$. The inset is a partial enlarged view at the very beginning time region. (b) $\sigma(t)$ rescaled by $\sigma_0 = \sigma(200)$.

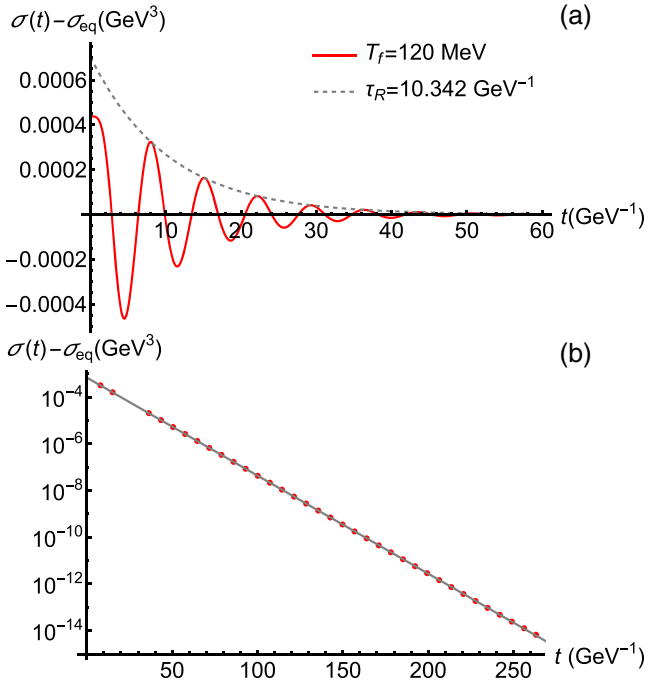

FIG. 2. (a) Relaxation process of sigma condensate, with initial state at $T_i = 110$ MeV and final equilibrium temperature at $T_f = 120$ MeV. (b) Envelope of the sigma condensate is fitted with the local maximum values of the oscillation attenuation curve of sigma condensate and the relaxation time $\tau_R = 10.342\ \mathrm{GeV}^{-1}$.

Therefore, we numerically verified that the relaxation is described by the linear response function Eqs. (12) and (13), and the relaxation time is related to the distance deviated from the critical temperature $\epsilon = T_f - T_c$ in the soft-wall model.[3]

2. Critical slowing-down

In the thermodynamic limit, it is well known that the critical slowing-down arises at the critical point, since the correlation length is getting divergent, as well as the relaxation time. However, this nonequilibrium phenomenon in the holographic QCD still lacks sufficient investigations. In this section, we will verify the critical slowing-down phenomenon with the dynamical evolution of the order parameter $\sigma(t)$ in the soft-wall model.

In the critical region (near the critical point), the correlation length ξ should satisfy the scaling hypothesis [82],

$$\xi(\epsilon, m_q, t) = b\xi(\epsilon b^{1/\nu}, m_q b^{\beta\delta/\nu}, tb^{-z}), \tag{14}$$

with an additional length rescaling factor b and static critical exponents β, ν, and δ. From Eq. (14), it is implicated that the sigma condensate satisfies

$$\sigma(\epsilon, m_q, t) = b^{-\beta/\nu}\sigma(\epsilon b^{1/\nu}, m_q b^{\beta\delta/\nu}, tb^{-z}), \tag{15}$$

and the relaxation time τ_R behaves as

$$\tau_R(\epsilon, m_q, t) = b^z\tau_R(\epsilon b^{1/\nu}, m_q b^{\beta\delta/\nu}, tb^{-z}). \tag{16}$$

After choosing particular scaling parameters m_q and ϵ, the corresponding scaling forms can be derived and the leading orders of the scaling forms, respectively, behave as

$$\xi \sim m_q^{-\nu/\beta\delta}, \qquad \sigma \sim m_q^{1/\delta}, \qquad \tau_R \sim m_q^{-\nu z/\beta\delta}, \tag{17a}$$

$$\xi \sim \epsilon^{-\nu}, \qquad \sigma \sim \epsilon^{\beta}, \qquad \tau_R \sim \epsilon^{-\nu z}. \tag{17b}$$

Those static critical exponents β, δ, and ν, have been obtained numerically and analytically in Refs. [55,74] with the soft-wall model. However, to describe the evolution of thermalization, an additional dynamic critical exponent z is required. From Eq. (15), one can obtain the scaling form in terms of t as

$$\sigma(t) = t^{-\beta/\nu z} f_{\mathrm{th}}(\epsilon t^{1/\nu z}, m_q t^{\beta\delta/\nu z}), \tag{18}$$

[3]The relaxation time also is a function of quark mass and other external parameters.

with the scaling function $f_{\rm th}$. So that the sigma condensate decays as a power law of the form

$$\sigma(t) = t^{-\beta/\nu z} f_{\rm th}(0,0) \propto t^{-\beta/\nu z}, \tag{19}$$

at the critical point, $\epsilon = 0$ and $m_q = 0$. It means that infinite time is needed to recover the equilibrium state $\sigma = 0$ at the critical point, which is the famous critical slowing-down phenomena.

We adopt four cases; they begin with the same initial sigma condensate. As verified in the last subsection, the initial values have no effect on the late time relaxation process, we only take a specific case of $\sigma_0 = 10^{-2}$ GeV^3 as an example. Then, one can quench the initial state to different final temperatures, $T_f = 157$, 159, 161, and 163 MeV, as shown in Fig. 3(a). From Eq. (13), one has the slope of the semilogarithmic curve corresponding to the inverse of the relaxation time. By fitting the data, we obtain $\tau_R = 3.960$, 6.929, 14.541, and 113.964 GeV^{-1} for $T_f = 157$, 159, 161, and 163 MeV, respectively. Varying the final temperature T_f in the condensed phase, the relaxation time increases with T_f. On the other hand, the relaxation of sigma condensate in the chiral symmetry restored phase is also shown in Fig. 3(b). We extract the relaxation time $\tau_R = 980.566$, 111.205, 20.177, and 6.092 GeV^{-1} for $T_f = 163.4$, 164, 167, and 175 MeV, respectively. The relaxation time decreases with the increasing temperature for $T_f > T_c$. Therefore, the relaxation time diverges either approaching to or receding from T_c.

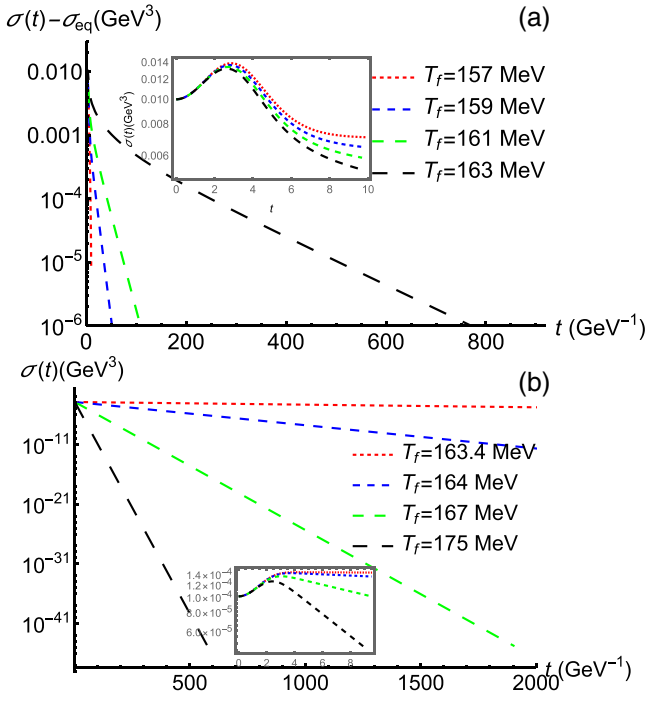

FIG. 3. Evolution of sigma condensate $\sigma(t)$ with different final temperatures T_f. (a) Time dependence of $\sigma(t) - \sigma_{\rm eq}$ with the same initial state $\sigma_0 = 10^{-2}$ GeV^3 quenched to different final temperatures T_f in the ordered phase. (b) Time dependence of $\sigma(t)$ with the same initial state $\sigma_0 = 10^{-4}$ GeV^3 quenched to different final temperatures T_f in the disordered phase.

Furthermore, we show extracted values of relaxation time at different temperatures in Fig. 4. The result shows that the relaxation time diverges at the critical temperature. When the system is a certain distance deviation from the critical point, the relaxation of the sigma condensation decreases exponentially, satisfying Eq. (13) with a particular relaxation time τ_R. As shown in Fig. 4(b), when ϵ approaches zero, the relaxation time behaves as the power-law divergence form in Eq. (17b). We fitted out the combination exponents $-\nu z = -1.04$ and -1.02 for the ordered phase and disordered phase, respectively. Since $\nu = 1/2$, we have $z \approx 2.08$ and 2.04. Except for the correlation time, we can study the critical slowing-down phenomena directly from the order parameter. As shown in Fig. 5(a), as examples, we have three different evolution curves of $\sigma(t)$ with different initial states quenched to the critical point. These different initial states are initial temperature $T_i = 100$ MeV, initial quark mass $m_i = 3.22$ MeV, and initial sigma condensate $\sigma_i = 10^{-2}$ GeV^3. After a very initial time stage, which mainly depends on the initial configurations and the microscopic details, the sigma condensate relaxes to the

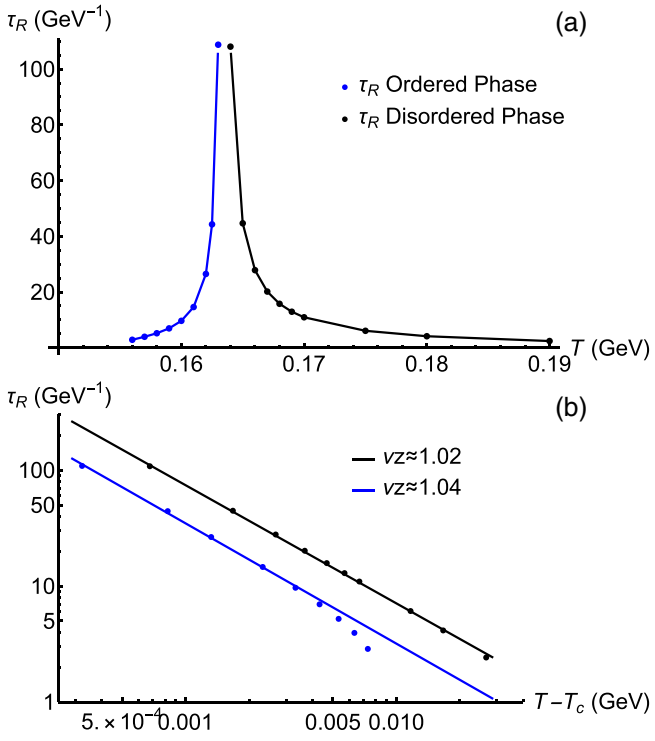

FIG. 4. (a) Relaxation time constant τ_R as a function of temperature. (b) Fitting the relaxation time constants with Eq. (17b).

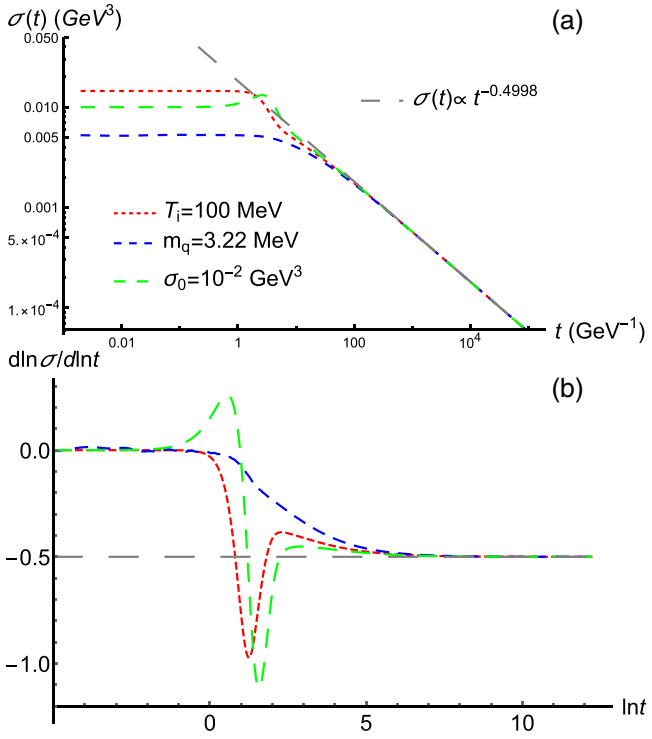

FIG. 5. (a) Time-dependent relaxation of σ quenched to the critical temperature with different initial sates. (b) Time-dependent evolution of $d\ln t/dt$.

equilibrium state in an extremely long time, as shown in Fig. 5(b).[4] The slope of $\sigma(t)$ in the log-log plot is about a constant value -0.4998 at the long time relaxation stage. From Eq. (19), it yields $-\beta/\nu z \approx -0.4998$. Thus, the dynamic exponent $z \approx 2.0008$, which is consistent with the result obtained from the scaling of the relaxation time. According to the classification in Ref. [84], the soft-wall model belongs to model A.[5]

B. The relation between the thermalization and QNM

At finite temperature, the Lorentz symmetry is broken, and the real part of the dispersion relation would behave as

$$\{\mathrm{Re}[\omega(\mathbf{p})]\}^2 = u_\pi^2(\mathbf{p}^2 + m_{\mathrm{scr}}^2), \tag{20}$$

where u_π is the pion velocity, m_{scr} is the screening mass that satisfies $\mathbf{p}^2 = -m_{\mathrm{scr}}^2$ at $\omega = 0$, and $m_{\mathrm{pole}} = \mathrm{Re}[\omega(0)] = u_\pi m_{\mathrm{scr}}$ is the pole mass at $\mathbf{p} = 0$ [85,86].

[4]During the review process, it is interesting to see that the recent study in holographic superfluid shows a similar behavior [83], though the symmetries considered in the two systems are different.

[5]Since the critical slowing-down, it is available to determine the critical temperature with scaling behaviors of the relaxation time or the sigma condensate. However, the critical temperature with extremely high accuracy is obtained through the static method proposed in Refs. [56,74].

The quasinormal mode is the oscillation mode of the perturbation of the background. The QNM frequency ω_0 corresponds to the pole of the two-point Green's function at $\mathbf{p} = 0$ [87]. Under the framework of holographic duality, the real and imaginary part of ω_0 correspond to the pole mass m_{pole} and the thermal width Γ [88]. We have already verified these relationships ($m_{\mathrm{pole}} = \mathrm{Re}[\omega_0]$ and $\Gamma/2 = -\mathrm{Im}[\omega_0]$) in the soft-wall AdS/QCD model in our previous work [55]. In that work, we also talk about the screening mass m_{scr} (inverse of the correlation length ξ^{-1}). A particular momentum satisfying $\mathbf{p}_0^2 + m_{\mathrm{scr}}^2 = 0$ corresponds to the pole of the two-point retarded Green's function at $\omega = 0$.

In this section, we will study the relationships among the relaxation time, correlation length, screening mass, and QNM frequency. For completeness, we briefly review the derivations of the retarded Green's function of the scalar mode; more details of the derivation can be found in Ref. [87]. The perturbation action of the scalar sector is

$$S_\sigma = \frac{1}{2}\int dx^5 \sqrt{g} e^{-\Phi}\Big[g^{\mu\nu}\partial_\mu S \partial_\nu S + g^{rr}(\partial_r S)^2 - m_5^2 S^2 - \frac{3\lambda}{2}\chi^2 S^2\Big]. \tag{21}$$

Then, we can derive the EOM for the scalar meson S as

$$S'' + \left(3A' + \frac{f'}{f} - \Phi'\right)S' + \left(\frac{\omega^2}{f^2} - \frac{p^2}{f} - \frac{2m_5^2 + 3\lambda\chi^2}{2f}A'^2\right)S = 0, \tag{22}$$

which is transformed into the momentum space $(\omega, \mathbf{p})$. For simplicity, we let $\mathbf{p}$ along a particular x_1 direction $\mathbf{p} = (p, 0, 0)$.

Near the boundary at $r = 0$, one can obtain the boundary asymptotic expansion as

$$S(r) = s_1 r + s_3 r^3 + \cdots, \tag{23}$$

with two integral constants s_1 and s_3. According to the holographic dictionary, one has s_1 corresponding to the extra source J_s. The incoming wave condition at the horizon $r = r_h$ is

$$S(r) \sim (r - r_h)^{-i\omega t/(4\pi T)}. \tag{24}$$

Combining these conditions, we numerically solve the EOM (22) though the so-called "shooting method" [56,79].

Following the prescription in Ref. [87], one has the retarded Green's function of S proportional to the ratio of s_1 and s_3,

$$G_s(\omega, p) \sim \frac{s_3(\omega, p)}{s_1(\omega, p)}. \tag{25}$$

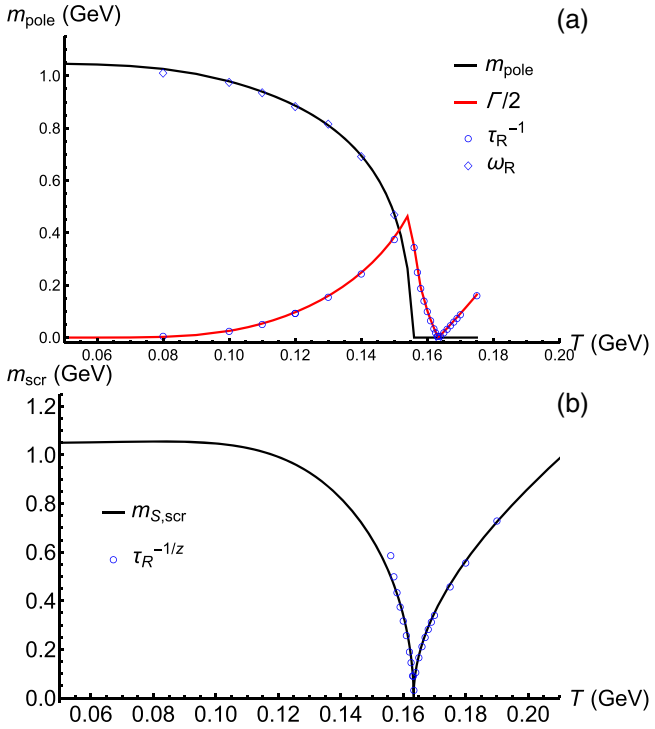

FIG. 6. (a) Comparison between the thermal width and the relaxation time, pole mass, and relaxation frequency. It is shown that $\Gamma_S/2 \approx \tau_R^{-1}$ and $m_{\rm pole} \approx \omega_R$. (b) Comparison between the screening mass and the relaxation time. In the critical region, it is shown that $m_{scr} = \xi^{-1} \approx k\tau_R^{-1/z}$ with a scalar factor $k \approx 2.47444 T_c^{1/2}$ in the ordered phase and $k \approx 2.82086 T_c^{1/2}$ in the disordered phase.

From Eq. (25), we know that the pole of the two-point retarded Green's function is equivalent to $s_1(\omega, p) = 0$. To obtain the pole mass $m_{\rm pole}$ and the thermal width Γ, we need to solve $s_1(\omega, 0) = 0$ and label the solution of the frequency as $\omega = \omega_0$. As to the screening mass $m_{\rm scr}$, we should solve $s_1(0, p) = 0$ and label the solution of the momentum as $p = p_0$.

We show the numerical results of pole mass,[6] thermal width, and the screening mass in Fig. 6(a) and the screening mass and the relaxation time in Fig. 6(b). The thermal width curve collapses with the curve of the inverse of the relaxation time. It means that the inverse of the thermal width can be identified as the relaxation time, i.e., $\Gamma/2 \approx 1/\tau_R$. As shown in Figs. 1 and 2, the value of the sigma condensate is varying with time in the relaxation process. More importantly, the absolute value of the sigma condensate departing from the equilibrium value is very small and approaching zero. It means that the whole relaxation process can be regarded as a slight perturbation on the equilibrium state. From the aspect of the scalar meson, it is enough to only consider up to the quadratic terms in the perturbation action (21). That would be the reason why the relaxation mode is well consistent with the scalar meson mode. As shown in Fig. 6(b), based on Eq. (17b), it is verified that the scaling mass and the relaxation time satisfy the relation $m_{\rm scr} = \xi^{-1} \approx k\tau_R^{-1/2}$ in the critical region with k a fitting parameter. In our numerical results, the fitting results are $k \approx 2.47444 T_c^{1/2}$ in the ordered phase and $k \approx 2.82086 T_c^{1/2}$ in the disordered phase.

[6]We remind the reader that, at low temperatures, the finite pole mass induces oscillations along with the relaxation evolution, as the case shown in Fig. 2.

IV. PRETHERMALIZATION

Governed by the timescales, the nonequilibrium process can be naturally divided into three stages, including the microscopic timescale dominated prescaling stage at the very beginning period, the prethermalization in the intermediate time, and the long time thermalization. The thermalization stage has been studied in the last section. Here, we will focus on the short time dynamics arising in the intermediate time.

A. Quench protocols

To clearly reveal the short time dynamics, we have a sketch for the quenching protocols. In the nonequilibrium evolution, the external parameters change with time,

$$R(t) \equiv (T(t), m(t)). \tag{26}$$

The initial state of the system is elaborately prepared, $R(t = 0) \equiv R_i = (T_i, m_i)$. Eventually, the system is quenched to the critical region, $R_f \equiv R(t \to +\infty) = (T_f, m_q)$. As shown in Fig. 7(a), three different initial states will be considered. Those are extremely high

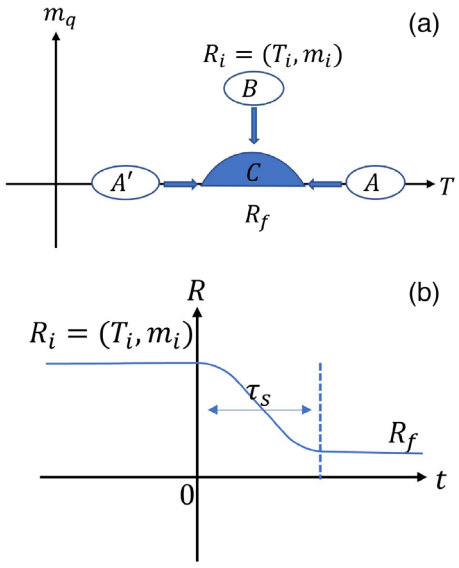

FIG. 7. (a) Schematic diagram of quench protocols. (b) Time dependence of the external parameters $R(t)$.

temperature with a finite sigma condensate ($A \to C$), finite quark mass ($B \to C$), and the equilibrium state in the ordered phase ($A' \to C$). The changing of the external parameters is shown in Fig. 7(b). To quench from R_i at $t = 0$ to R_f is within a finite timescale τ_Q. In this work, we only consider the sudden quench case, i.e., $\tau_Q \to 0$, so that

$$R(t) = R_i + \theta(t)(R_f - R_i), \tag{27}$$

with $\theta(t)$ as the step function.

B. Short time scaling

In Sec. III, we have studied the properties in the limit of thermalization. In the asymptotic long time stage, all the initial state information has been washed out. It is shown that the system reaches the equilibrium thermal state, which only depends on the final external parameters R_f. However, in the prethermalization stage, the evolution is expected to depend on the initial parameters, $R_i = (T_i, m_i)$. Inspired by the short time scaling in the condensed matter model [21–24], we have a suggested a scaling hypothesis for the sigma condensate,

$$\sigma(R_i, \epsilon, m_q, t) = b^{-\beta/\nu}\sigma(R_i(b), \epsilon b^{1/\nu}, m_q b^{\beta\delta/\nu}, tb^{-z}), \tag{28}$$

with a scaling length parameter b. $R_i(b)$ is the initial parameters rescaled by b. As a result of the memory of the initial state, the scaling is proposed to employ a new exponent x, and so Eq. (28) becomes

$$\sigma(\epsilon_i, m_i, \epsilon, m_q, t) = b^{-\beta/\nu}\sigma(\epsilon_i b^{x/\nu}, m_i b^{x\beta\delta/\nu}, \epsilon b^{1/\nu}, m_q b^{\beta\delta/\nu}, tb^{-z}). \tag{29}$$

Near the critical point, the equilibrium sigma condensate relates to the distance to the critical point with $\sigma \sim \epsilon^\beta$, so that one obtains

$$\sigma(\sigma_i, m_i, \epsilon, m_q, t) = b^{-\beta/\nu}\sigma(\sigma_i b^{x\beta/\nu}, m_i b^{x\beta\delta/\nu}, \epsilon b^{1/\nu}, m_q b^{\beta\delta/\nu}, tb^{-z}). \tag{30}$$

1. Quench from the disordered phase

In the chiral limit, when the temperature is above the critical temperature $T > T_c$, the solution of $\chi(z)$ is exactly equal to 0. Thus the sigma condensate $\sigma = 0$. To realize the nonequilibrium evolution from the disordered phase to the critical region, a finite initial condensate σ_i is necessary for the initial state. From the asymptotic solution of $\chi(r)$ in Eq. (4), we know that m_q and σ are two integral constants for this solution. Since the chiral limit $m_q = 0$, the leading term of this solution becomes $(\sigma/\gamma)r^3$. In addition, $r_h = 1/T$ is very small at high temperature. It means that $r \le r_h$ is very small. Therefore, when $T_i > T_c$, we can take the asymptotic solution as an approximation of the initial state,

$$\chi(r) = \frac{\sigma_i}{\gamma} r^3. \tag{31}$$

First, we consider the sudden quench to the critical point, i.e., $\epsilon = T_f - T_c = 0$ and $m_q = 0$. To derive the specific scaling form in terms of t, one can let $tb^{-z} = t_{\rm pre}$ where $t_{\rm pre}$ is a microscopic timescale. $t_{\rm pre}$ marks the moment when the universal prethermalization stage begins. Then, from Eq. (30), we have

$$\sigma(\sigma_i, 0, 0, 0, t) = t^{\frac{-\beta}{\nu z}}\sigma\left[\sigma_i (t/t_{\rm pre})^{\frac{x\beta}{\nu z}}, 0, 0, 0, t_{\rm pre}\right]. \tag{32}$$

One can define a new scaling function

$$f_t(\sigma_i t^{x\beta}/\nu z) \equiv \sigma\left[\sigma_i (t/t_{\rm pre})^{x\beta/\nu z}, 0, 0, 0, t_{\rm pre}\right]. \tag{33}$$

Therefore, one can obtain the following scaling form in terms of t as

$$\sigma(\sigma_i, t) = t^{-\beta/\nu z} f_t(\sigma_i t^{x\beta/\nu z}). \tag{34}$$

In the long time region, the system evolves into the thermalization stage and $\sigma_i t^{x\beta/\nu z} \gg 1$, so that $f_t = \text{const}$ and $\sigma(\sigma_i, t) \propto t^{-\beta/\nu z}$, which has been verified in Sec. III. In the short time region, one has $t \ll t_{\rm th} \propto \sigma_i^{-\nu z/x\beta}$. The time scalar $t_{\rm th}$ marks the system crossover to the thermalization regime. Note that t is often referred to as the waiting time. In this period, the magnitude of sigma condensates has not varied too much, compared to σ_i, so that f_t is dominated by its linear term. It implies that

$$\sigma(\sigma_i, t) \propto \sigma_i t^{(x-1)\beta/\nu z}. \tag{35}$$

Additionally, the general scaling form in terms of σ_i is presented by Eq. (30) as

$$\sigma(\sigma_i, t) = \sigma_i^{1/x} f_{\sigma_i}(t\sigma_i^{z\nu/x\beta}), \tag{36}$$

with a scaling function f_{σ_i}. In the short time, one has $f_{\sigma_i} \propto \sigma_i^{(x-1)/x} t^{(x-1)\beta/\nu z}$ to guarantee that $\sigma(\sigma_i, t)$ satisfies Eq. (35). One can define the short time dynamic (dynamic initial-slip) exponent $\theta \equiv (x-1)\beta/\nu z$ to characterize the universal short time behavior.

In Fig. 8(a), there is obvious difference on the order of the magnitude of initial σ_i, but the evolution curves share the same tendency and all can be separated into three stages. The intermediate stage is the period in which the short time dynamic appears. Through numerically fitting the data according to Eq. (35) as shown in Fig. 8(b), we have $\theta \approx 0$ or $x \approx 1$. With the short time dynamical critical exponent, the curves with different initial states can be

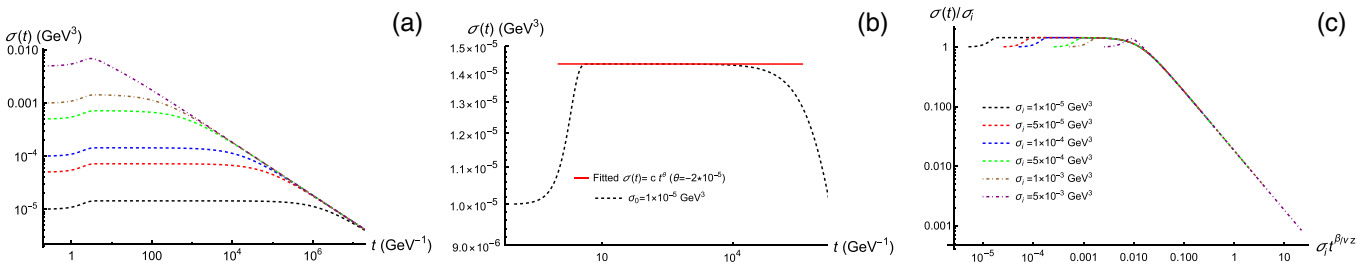

FIG. 8. (a) Evolution of the sigma condensate with different initial sigma condensate values sudden quenched to the critical point. (b) Fitting the intermediate time with Eq. (35), one gets the short time dynamic exponent $\theta = -2 \times 10^{-5}$. (c) Scaling the evolution curves of the sigma condensate in (a) based on Eq. (36).

completely scaled by Eq. (36) as shown in Fig. 8(c). Therefore, it is verified that the universal short time behavior with the exponent $\theta = 0$ arises in the prethermalization stage. It implies that a smaller initial sigma condensate leads to a longer duration of the prethermalization stage.

If the final state is slightly deviated from the critical point, the evolution still can emerge as the universal short time behavior. Similar to the derivation of scaling form in Eq. (34), one can derive the corresponding scaling form in terms of t as

$$\sigma(\sigma_i, \epsilon, m_q, t) = t^{-\beta/\nu z} f_t(\sigma_i t^{x\beta/\nu z}, \epsilon t^{1/\nu z}, m_q t^{\beta\delta/\nu z}). \quad (37)$$

One can also have the scaling form in terms of σ_i as

$$\sigma(\sigma_i, \epsilon, m_q, t) = \sigma_i^{1/x} f_{\sigma_i}(\epsilon \sigma_i^{-1/x\beta}, m_q \sigma_i^{-\delta/x}, t\sigma_i^{\nu z/x\beta}). \quad (38)$$

When the final state is $R_f = (T_f, 0)$ with $\epsilon = T_f - T_c \neq 0$, the system will relax to the final equilibrium state with finite time at $\sigma \propto \epsilon^{\beta}$ in the ordered phase, as shown in Fig. 9, or at $\sigma = 0$ in the disordered phase, as shown in Fig. 10. In Eq. (38), the scaling function f_{σ_i} has three variables. For simplicity, we use the projection method to analyze the multivariate scaling behavior. We get the evolution curves in Figs. 9(a) and 9(b) by fixing $-\epsilon\sigma_i^{-1/\beta} = 3323$ and 92, respectively. To verify the scaling function, based on Eq. (38), we plot $\sigma(t)/\sigma_i^{1/x}$ versus $\sigma_i t^{\beta/\nu z}$ in Fig. 9(c). Since the short time dynamic exponent $\theta = 0$, the curves overlap and behavior is as a plateau in the prethermalization stage. In the long time limit, the curves overlap and show as horizontal lines at different values because of different fixing values. Note that the different fixing values only change the crossover position and have no impact on the short time scaling behavior.

In another case, we let the final state $R_f = (0, m_q)$ and fix $m_q \sigma_i^{-\delta} = 3 \times 10^{-6}$. In Fig. 11(a), the prethermalization stage arises after the microscopic-scale dominant region. Then the system crosses to the long time thermalization stage. Finally, the system relaxes to the steady state and $\sigma \propto m_q^{1/\delta}$. Scaling the data according to the scaling form in

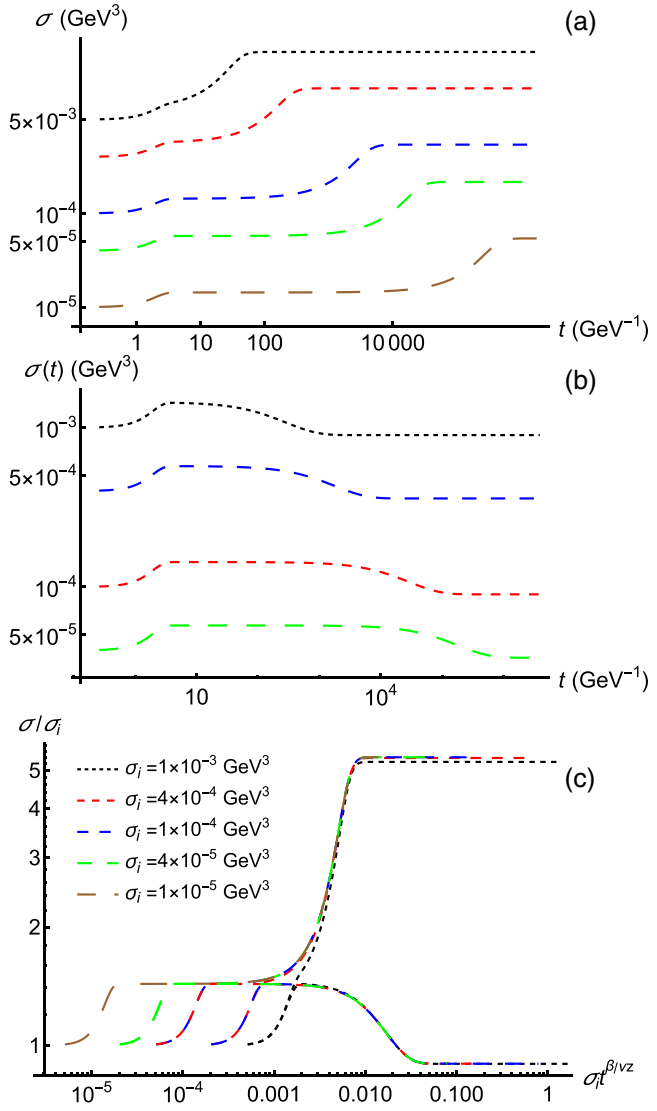

FIG. 9. Evolution curves of sigma condensate with (a) $-\epsilon\sigma_i^{-1/\beta} = 3323$ and (b) $-\epsilon\sigma_i^{-1/\beta} = 92$. (c) Scaling the evolution curves of sigma condensate in (a) and (b) based on Eq. (38).

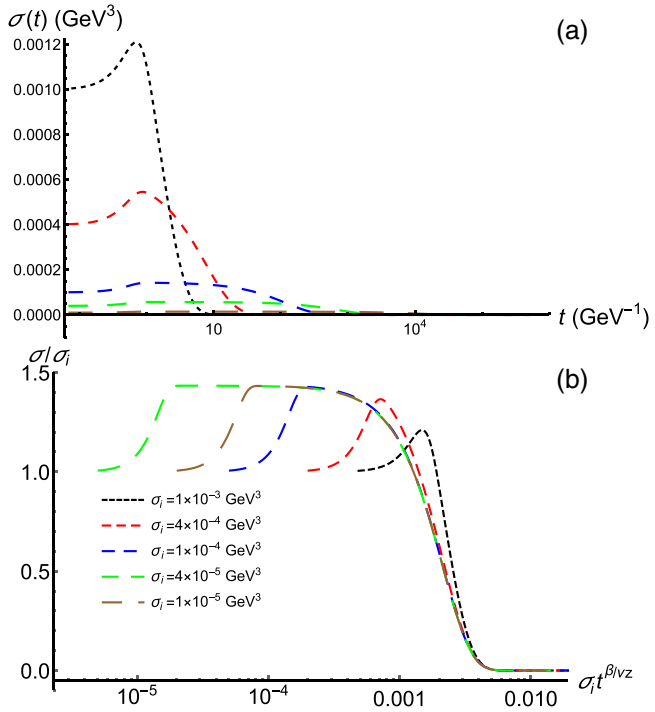

FIG. 10. (a) Evolution curves of sigma condensate with $\epsilon\sigma_i^{-1/\beta} = 16677$. (b) Scaling the evolution curves of sigma condensate in (a) based on Eq. (38).

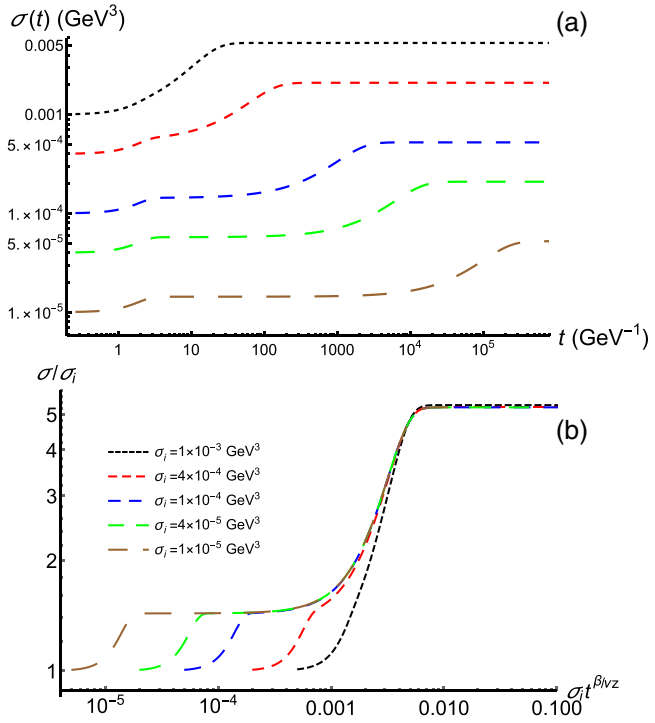

FIG. 11. (a) Evolution curves of sigma condensate with $m_q\sigma_i^{-\delta} = 3 \times 10^6$. (b) Scaling the evolution curves of sigma condensate in (a) based on Eq. (38).

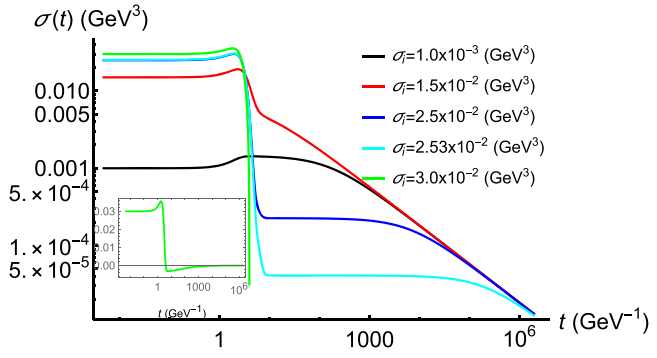

FIG. 12. Initial state dependence of the sigma condensate evolution $\sigma_i \gtrsim \sigma_{\rm sat}$.

Eq. (38), we obtain overlapped curves in Fig. 11(b). These numerical analyses indicate that the scaling function f_{σ_i} is well verified through the projection method.

In above analyses, the short time dynamic and the thermalization are realized with small initial sigma condensates. What if the magnitudes of the initial sigma condensate are close to or larger than the saturated value? Generally, in the small initial sigma condensate, before the universal short time dynamic, there are two particular properties in evolution. On the one hand, it is a nonuniversal period. On the other hand, this period is about in $0 \le t \le t_{\rm pre} \approx 2\pi T_f$. As shown in Fig. 12, we find that when σ_i is almost equal to or larger than $\sigma_{\rm sat}$, $\sigma(t)$ show a steep decrease approximately at $t_{\rm pre}$. If $\sigma_i \lesssim 2.54 \times 10^{-2}$ GeV^3, $\sigma(t)$ drops to a "prethermalization" state.[7] However, if σ_i are roughly larger than 2.54×10^{-2} GeV^3, for example when $\sigma_i = 3.0 \times 10^{-2}$ GeV^3, the sigma condensate drops to a negative value and approaches zero from the bottom, as shown in the inset of Fig. 12.

2. Quench from the ordered phase

As in the schematic program shown in Fig. 7, we will also study the short time dynamics from $A' \to C$ and $B \to C$. Without considering the high orders, the five-dimensional scalar field behaves as $\chi(r) \propto r^3$ in the critical region. It is interesting to explore whether the scaling behavior in this case is the same as the case of $A \to C$.

One can apply the initial state at $R_i = (\epsilon_i, m_i)$ and sudden quench the system to the critical point. By choosing the particular scaling, the scaling form of Eq. (29) transforms to

$$\sigma(\epsilon_i, m_i, t) = t^{-\beta/\nu z} f_t(\epsilon_i t^{x/\nu z}, m_i t^{x\beta\delta/\nu z}), \qquad (39)$$

[7]It might be not a real prethermalization stage, but behaves as a prethermalization.

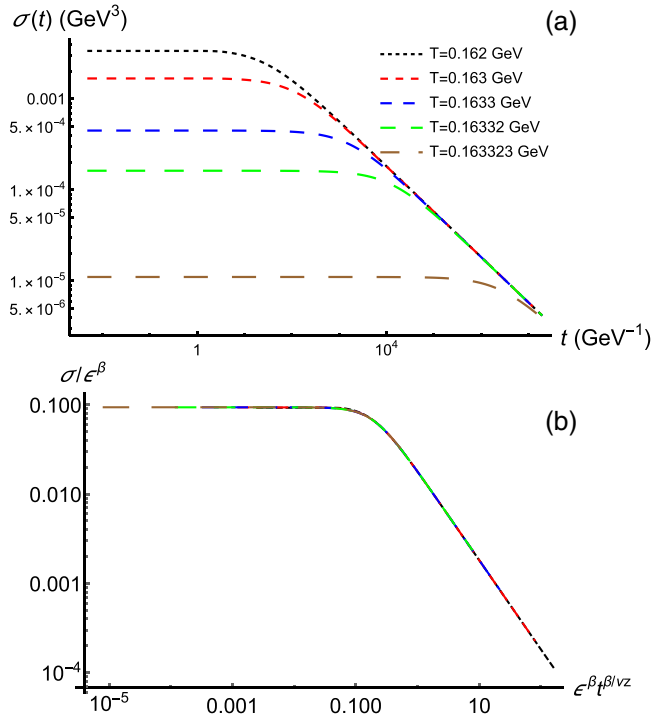

FIG. 13. (a) Evolution curves of sigma condensate with different initial temperature. (b) Scaling the evolution curves of sigma condensate in (a) based on Eq. (40a).

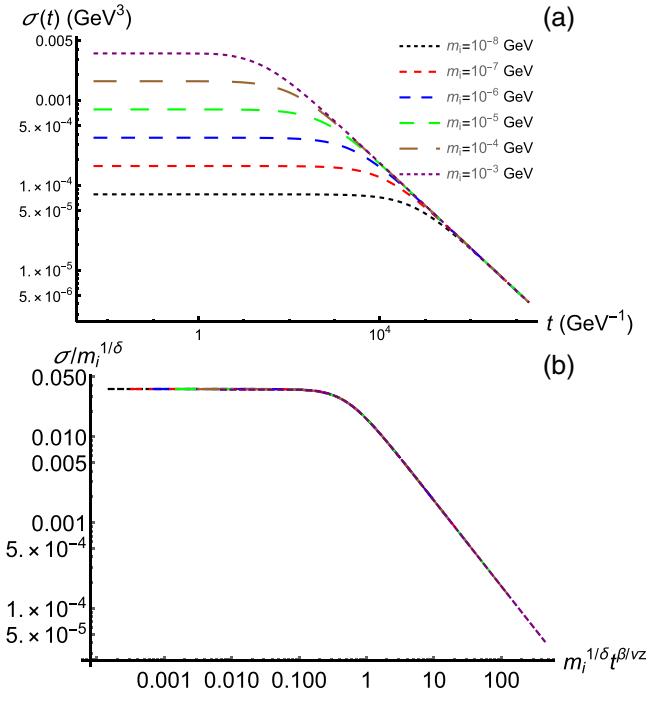

FIG. 14. (a) Evolution curves of sigma condensate with different initial quark mass. (b) Scaling the evolution curves of sigma condensate in (a) based on Eq. (40b).

and

$$\sigma(\epsilon_i, m_i, t) = \epsilon_i^{\beta/x} f_{\epsilon_i}(m_i \epsilon^{-\beta\delta}, t\epsilon_i^{\nu z/x}), \tag{40a}$$

$$\sigma(\epsilon_i, m_i, t) = m_i^{1/\delta x} f_{m_i}(\epsilon_i m_i^{-1/\beta\delta}, t m_i^{\nu z/x\beta\delta}). \tag{40b}$$

Because of the complexity of considering finite ϵ_i and m_i simultaneously, we separately consider either finite ϵ_i or m_i at once. When $R_i = (\epsilon_i, 0)$, $\sigma(t)$ should behave as $\sigma \propto \epsilon_i^\beta$ in the prethermalization stage, so that $f_t \propto (\epsilon_i t^{x/\nu z})^\beta$. Thus, one has the leading scaling term as

$$\sigma \propto \epsilon_i^\beta t^{(x-1)\beta/\nu z} = \epsilon_i^\beta t^\theta. \tag{41}$$

In the long time region, the scaling function f_t must reduce to a constant, so that the evolution of the sigma condensate is reduced to the critical slowing-down scaling $\sigma \propto t^{-\beta/\nu z}$, which has been studied in Sec. III A 2. The numerical results are shown in Fig. 13(a). The evolution has two different features: the prethermalization and the thermalization stages. In Fig. 13(b), according to Eq. (40a), by scaling the $\sigma(t)$ with ϵ_i^β, the curves of $\sigma(t)/\epsilon_i^\beta$ overlap as a function of $\epsilon_i^\beta t^{\beta/\nu z}$.

Similarly, we let $R_i = (0, m_i)$ and study the scaling function in Eq. (40b). Along with the evolution, first, sigma condensate behaves as $\sigma(t) \propto m_i^{1/\delta} t^{(x-1)\beta/\nu z} = m_i^{1/\delta} t^\theta$ in the prethermalization stage, then crosses to $\sigma(t) \propto t^{-\beta/\nu z}$ in the thermalization stage. These scaling predictions are verified in Fig. 14. In Fig. 13(a), it is the original data for $\sigma(t)$. The curves have the prethermalization and the thermalization stages and their crossover. As predicted by the scaling form in Eq. (40b), the $\sigma(t)/m_i^{1/\delta}$ versus $m_i^{1/\delta} t^{\beta/\nu z}$ curves overlap each other in Fig. 14.

It seems that the evolution in Figs. 13 and 14 does not have obvious boundaries between the prescaling and prethermalization stages, which are primarily different from Fig. 8. To analyze the difference between them, we compare the evaluations of sigma condensate $\sigma(t)$ and the second derivation of the chiral field with respect to $r\chi''(r)$. For convenience of numerical calculation, we have a coordinate transform in Eq. (11),

$$u = r/r_h, \qquad \tilde{v} = v/r_h. \tag{42}$$

In Fig. 15, we show the numerical results of $\sigma(t)$ and $\chi''(u)/\sigma(t=0)$ obtained from the quench paths $A \to C$ and $A' \to C$ with equal initial sigma condensate in Fig. 14. The sigma condensation increases in the very beginning nonuniversal period in the case of $A \to C$. However, the sigma condensation almost keeps invariant in the nonuniversal period in the case of $A' \to C$. From the aspect of $\chi''(u)/\sigma(t=0)$, in the prescaling stage, in case $A \to C$, $\chi''(u)/\sigma(t=0)$ has a changing process from a constant to a

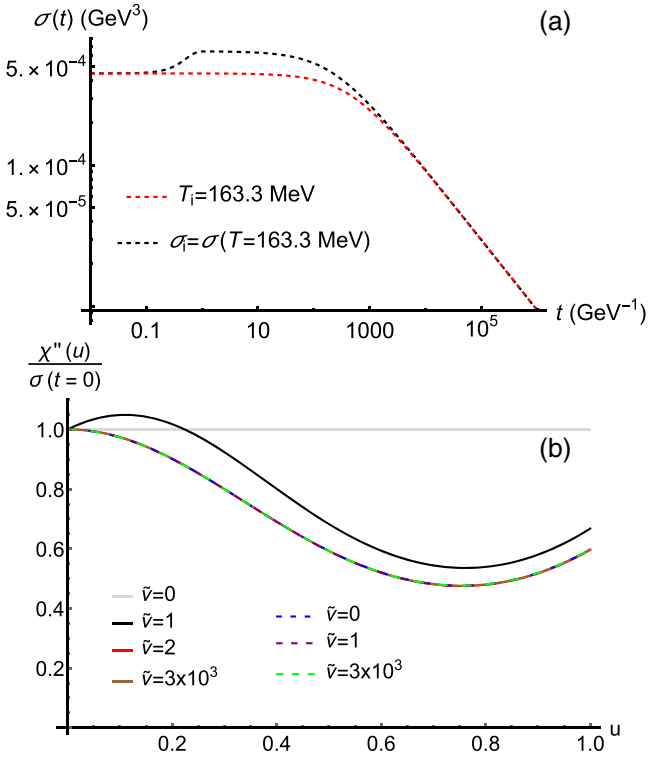

FIG. 15. (a) Time dependence of $\sigma(t)$ with equal σ_i through different quenching protocols, $A \to C$ and $A' \to C$. (b) Curves of $\chi''(u)/\sigma(t=0)$ at different $\tilde{\nu}$.

time-independent function. In case $A' \to C, \chi''(u)/\sigma(t=0)$ is always a time-independent function.

It is interesting that the ratio is stable in the prethermalization stage and equal the values in the thermalization stage. It means that the time-dependent term and u-dependent part are decoupled in Eq. (11). To some extent, even though the scaling form in prethermalization is totally different from the thermalization, there are some particular physical quantities that behave like the (quasi)equilibrium state. Furthermore, as a result of the decoupling of t and u, if the sigma condensate satisfies the power-law scaling $\sigma(t) \propto t^{-a}$ with $a > 0$, i.e., $\sigma(\tilde{v}) \propto \tilde{v}^{-a}$ for $t = \tilde{v}\pi T$ at $r = 0$, one has $\chi(\tilde{v}, u) = \sigma(\tilde{v})g(u)$. From Eq. (A1), one can derive $-a - 1 = -3a$, thus $a = 1/2$, with dimension analysis. Moreover, there is another solution, $\sigma(t) \propto t^0$. These two solutions correspond to the thermalization and prethermalization, respectively.

V. CONCLUSIONS AND DISCUSSIONS

The soft-wall AdS/QCD model provides an effective holographic framework to deal with the nonperturbative problems of QCD, especially for chiral symmetry breaking and restoration. Since the model contains information of the order parameter, it would be quite interesting to extend the previous equilibrium studies to nonequilibrium phase transition.

By quenching the system from initial states deviating from the equilibrium states, we solve the real-time evolution of chiral condensate in the two-flavor ($N_f = 2$) soft-wall AdS/QCD model. At this stage, we work in the probe limit, i.e., neglecting the backreaction to the background geometry. In this way, we are considering the thermalization of the system under an infinite heat bath.

It is shown that, at very low temperatures, the chiral condensate shows oscillating behaviors, while its amplitude decays exponentially with time. At higher temperatures, but still below T_c, the oscillation disappears and only the fast exponential damping is left. We compare the oscillating frequencies and the relaxation times with the complex frequency of quasinormal modes. It is found that they match with each other very well. Therefore, the late-time thermalization of the system could be described by the quasinormal modes. Furthermore, it is also found that the relaxation time would diverge when the temperature of the heat bath approaches T_c, showing a typical behavior of critical slowing-down. The exponential damping turns to a power law, and by fitting the late-time behavior, we get the dynamical critical exponent $z \approx 2.0$.

In addition to the late-time thermalization, it is more interesting to observe that, starting from a large class of initial states, the system would linger over a quasi-steady-state for a certain period of time before the thermalization, which is very similar to the interesting phenomenon named prethermalization in the QCD community. According to the extracted initial-slip exponent $\theta \approx 0$, it is observed that such quantity is still a mean-field value due to the large N suppression. Therefore, there are some important open issues that can be studied in the future. From a theoretical point of view, it is crucial to explore how to vary the initial conditions to realize the scenario of the nonthermal fixed point in the soft-wall AdS/QCD model and whether the collective modes of two out-of-equilibrium universalities, characterized by the NTFP and the initial-slip exponent, are the same.

In the prethermalized regime, θ arises as a new universal critical exponent, which forms as the memory of initial configurations. Taking into account the rapidly decayed magnetic field that is produced in the off-central heavy-ion collisions, the mass of charged particles, such as protons, is strongly altered by the magnetized environment, which presents as a unique scenario to study the short time dynamical scaling and its subsequent behaviors [27]. A prolonged stage also affects the estimation of rapidity distribution of the charged particles as a function of collision centrality in experimental measurements. A quantitative impact of the initial-slip exponent on the two- and higher-point correlation functions of protons remains to be evaluated.

Triggered by the forthcoming experimental measurements at high baryon chemical potentials, the description of fireballs created in low-energy collisions needs to be

contained the phase transition of the first order [89]. The corresponding time evolution has to be improved in two aspects. First, the soft-wall AdS/QCD model should extend to finite chemical potentials, where the first-order phase transition occurs and the phase boundary beyond the critical point is located [45]. Second, coupling with the baryon density, the chiral condensate is governed by the conservation law and its linear response is presented by the diffusive equation. The influence of the short time dynamical behaviors on the possible spinodal instability and other associated phenomena are under way and will be published elsewhere.

ACKNOWLEDGMENTS

We would like to thank the useful discussion with Yidian Chen, Song He, Mei Huang, Lang Yu, and Xinyang Wang. X. C. is supported by the National Natural Science Foundation of China under Grant No. 12275108 and the Fundamental Research Funds for the Central Universities under Grant No. 21622324. J. C. is supported by the start-up funding from Jiangxi Normal University under Grant No. 12021211. H. L. is supported by the National Natural Science Foundation of China under Grant No. 11405074. D. L. is supported by the National Natural Science Foundation of China under Grants No. 12275108, No. 12235016, and No. 11805084, the Phd. Start-up Fund of Natural Science Foundation of Guangdong Province under Grant No. 2018030310457, and the Guangdong Pearl River Talents Plan under Grant No. 2017GC010480.

APPENDIX: PSEUDOSPECTRAL METHOD

The pseudospectral method [79,80] is a very effective numerical method with high accuracy for solving the initial-value problem of the partial differential equation. The following is a brief overview to simulate the EOM in Eq. (A1) by the pseudospectral method.

First, we apply the variable substitution $v \to \tilde{v} \equiv v/r_h$ and $r \to u \equiv r/r_h$. Then Eq. (11) becomes

$$\begin{aligned} &2\partial_{\tilde{v}}\partial_u\chi(\tilde{v},u) - \left[\frac{3}{u} + \Phi'(u)\right]\partial_{\tilde{v}}\chi(\tilde{v},u) - f(u)\partial_u^2\chi(\tilde{v},u) \\ &\quad + \left[\frac{3}{u}f(u) + \Phi'(u)f(u) - f'(u)\right]\partial_u\chi(\tilde{v},u) \\ &\quad + \frac{1}{u^2}(m_5^2 + \frac{\lambda}{2}\chi(\tilde{v},u)^2)\chi(\tilde{v},u) = 0. \end{aligned} \tag{A1}$$

Generally, the function $\chi(r)$ can be expanded into the nodal expansion

$$\chi(u) = \sum_{i=0}^{N} \chi_i l_i(u), \tag{A2}$$

with

$$\begin{aligned} \chi_i &= \chi(u_i), \\ l_i(u) &= \prod_{i=0, i\neq j}^{N} \frac{u - u_i}{u_j - u_i}, \end{aligned}$$

where $\{u_i\}_{i=0}^N$ are the collocation points and $\{l_i\}_{i=0}^N$ are the basis functions. In this expansion, the undetermined parameters are directly the function values at the collocation points. For the optimal scenario, the collocation points or the grid points $\{u_i\}_{i=0}^N$ for the basis are given by the Chebyshev-Gauss-Lobatto points [90]. The discrete u in the interval [0, 1] is

$$u_i = \frac{1}{2}\left[1 - \cos\left(\frac{i-1}{N-1}\pi\right)\right], \tag{A3}$$

with $j = 1, 2, \ldots, N$. In this work, we choose $N = 60$. The derivative operator ∂_x is approximately replaced by a discrete finite difference derivative $\hat{D}$. At the point u_j, one obtains the p-order derivative as

$$\chi^{(p)}(u_j) = \hat{D}^{(p)}\chi(u_j) = \sum_{i=0}^{N} \chi_i l_i^{(p)}(u_j). \tag{A4}$$

In our calculation, the derivation is realized by employing the built-in "FiniteDifferenceDerivative" operator in *Mathematica*. Then, we get a series of equations in the form of

$$\partial_{\tilde{v}}\chi(\tilde{v}, u_i) = F[\hat{D}, u_i, \chi(\tilde{v}, u_i)], \tag{A5}$$

with $i = 1, 2, \ldots, N$. Thus, a second-order partial differential equation is transformed into the first-order ordinary differential equation. With prepared initial conditions $\chi(0, u_i) = \chi_0(u_i)$, it is straightforward that these equations are solved.

[1] I. Arsene *et al.* (BRAHMS Collaboration), Nucl. Phys. **A757**, 1 (2005).
[2] B. Berdnikov and K. Rajagopal, Phys. Rev. D **61**, 105017 (2000).
[3] J. Randrup, Phys. Rev. C **82**, 034902 (2010).
[4] B. P. Abbott *et al.* (LIGO Scientific and Virgo Collaborations), Phys. Rev. Lett. **116**, 061102 (2016).
[5] N. Barnaby, Z. Huang, L. Kofman, and D. Pogosyan, Phys. Rev. D **80**, 043501 (2009).
[6] I. Bloch, J. Dalibard, and W. Zwerger, Rev. Mod. Phys. **80**, 885 (2008).
[7] M. Ueda, Nat. Rev. Phys. **2**, 669 (2020).
[8] J. Berges, S. Borsanyi, and C. Wetterich, Phys. Rev. Lett. **93**, 142002 (2004).
[9] J. Berges, M. P. Heller, A. Mazeliauskas, and R. Venugopalan, Rev. Mod. Phys. **93**, 035003 (2021).
[10] M. Prüfer, P. Kunkel, H. Strobel, S. Lannig, D. Linnemann, C.-M. Schmied, J. Berges, T. Gasenzer, and M. K. Oberthaler, Nature (London) **563**, 217 (2018).
[11] S. Erne, R. Bücker, T. Gasenzer, J. Berges, and J. Schmiedmayer, Nature (London) **563**, 225 (2018).
[12] A. Piñeiro Orioli, K. Boguslavski, and J. Berges, Phys. Rev. D **92**, 025041 (2015).
[13] A. Chiocchetta, A. Gambassi, S. Diehl, and J. Marino, Phys. Rev. Lett. **118**, 135701 (2017).
[14] J. Berges, A. Rothkopf, and J. Schmidt, Phys. Rev. Lett. **101**, 041603 (2008).
[15] J. Berges and B. Wallisch, Phys. Rev. D **95**, 036016 (2017).
[16] J. Bonart, L. F. Cugliandolo, and A. Gambassi, J. Stat. Mech. (2012) P01014.
[17] P. Gagel, P. P. Orth, and J. Schmalian, Phys. Rev. Lett. **113**, 220401 (2014).
[18] M. Rigol, V. Dunjko, V. Yurovsky, and M. Olshanii, Phys. Rev. Lett. **98**, 050405 (2007).
[19] M. Kollar, F. A. Wolf, and M. Eckstein, Phys. Rev. B **84**, 054304 (2011).
[20] T. Mori, T. N. Ikeda, E. Kaminishi, and M. Ueda, J. Phys. B **51**, 112001 (2018).
[21] H. Janssen, B. Schaub, and B. Schmittmann, Z. Phys. B Condens. Matter **73**, 539 (1989).
[22] H. Schoeller, Eur. Phys. J. Special Topics **168**, 179 (2009).
[23] J. Berges, N. Tetradis, and C. Wetterich, Phys. Rep. **363**, 223 (2002).
[24] P. Gagel, P. P. Orth, and J. Schmalian, Phys. Rev. B **92**, 115121 (2015).
[25] L. M. Sieberer, M. Buchhold, and S. Diehl, Rep. Prog. Phys. **79**, 096001 (2016).
[26] W.-T. Deng and X.-G. Huang, Phys. Rev. C **85**, 044907 (2012).
[27] K. Xu, S. Shi, H. Zhang, D. Hou, J. Liao, and M. Huang, Phys. Lett. B **809**, 135706 (2020).
[28] D. E. Kharzeev, Prog. Part. Nucl. Phys. **75**, 133 (2014).
[29] M. A. Stephanov, Phys. Rev. Lett. **107**, 052301 (2011).
[30] X. An *et al.*, Nucl. Phys. **A1017**, 122343 (2022).
[31] G. Policastro, D. T. Son, and A. O. Starinets, Phys. Rev. Lett. **87**, 081601 (2001).
[32] A. Buchel and J. T. Liu, Phys. Rev. Lett. **93**, 090602 (2004).
[33] P. K. Kovtun, D. T. Son, and A. O. Starinets, Phys. Rev. Lett. **94**, 111601 (2005).
[34] P. K. Kovtun and A. O. Starinets, Phys. Rev. D **72**, 086009 (2005).
[35] P. M. Chesler, A. M. García-García, and H. Liu, Phys. Rev. X **5**, 021015 (2015).
[36] J. Sonner, A. del Campo, and W. H. Zurek, Nat. Commun. **6**, 7406 (2015).
[37] Y. Bu, M. Fujita, and S. Lin, Phys. Rev. D **101**, 026003 (2020).
[38] H. Liu and J. Sonner, Rep. Prog. Phys. **83**, 016001 (2019).
[39] C. Ewerz, T. Gasenzer, M. Karl, and A. Samberg, J. High Energy Phys. 05 (2015) 070.
[40] P. M. Chesler and L. G. Yaffe, Phys. Rev. Lett. **102**, 211601 (2009).
[41] P. M. Chesler and L. G. Yaffe, Phys. Rev. D **82**, 026006 (2010).
[42] K. Rajagopal, A. V. Sadofyev, and W. van der Schee, Phys. Rev. Lett. **116**, 211603 (2016).
[43] M. Atashi, K. Bitaghsir Fadafan, and G. Jafari, Eur. Phys. J. C **77**, 430 (2017).
[44] J. Casalderrey-Solana, M. P. Heller, D. Mateos, and W. van der Schee, Phys. Rev. Lett. **111**, 181601 (2013).
[45] R. Critelli, R. Rougemont, and J. Noronha, J. High Energy Phys. 12 (2017) 029.
[46] T. Ishii, E. Kiritsis, and C. Rosen, J. High Energy Phys. 08 (2015) 008.
[47] A. Karch, E. Katz, D. T. Son, and M. A. Stephanov, Phys. Rev. D **74**, 015005 (2006).
[48] T. M. Kelley, S. P. Bartz, and J. I. Kapusta, Phys. Rev. D **83**, 016002 (2011).
[49] Y.-Q. Sui, Y.-L. Wu, Z.-F. Xie, and Y.-B. Yang, Phys. Rev. D **81**, 014024 (2010).
[50] P. Colangelo, F. De Fazio, F. Giannuzzi, F. Jugeau, and S. Nicotri, Phys. Rev. D **78**, 055009 (2008).
[51] A. Ballon-Bayona and L. A. H. Mamani, Phys. Rev. D **102**, 026013 (2020).
[52] E. Folco Capossoli, M. A. Martín Contreras, D. Li, A. Vega, and H. Boschi-Filho, Chin. Phys. C **44**, 064104 (2020).
[53] D. Li, M. Huang, and Q.-S. Yan, Eur. Phys. J. C **73**, 2615 (2013).
[54] D. Li and M. Huang, J. High Energy Phys. 11 (2013) 088.
[55] X. Cao, S. Qiu, H. Liu, and D. Li, J. High Energy Phys. 08 (2021) 005.
[56] X. Cao, H. Liu, and D. Li, Phys. Rev. D **102**, 126014 (2020).
[57] M. Rinaldi, F. A. Ceccopieri, and V. Vento, Eur. Phys. J. C **82**, 626 (2022).
[58] S. S. Afonin and T. D. Solomko, Eur. Phys. J. C **82**, 195 (2022).
[59] S. Mamedov and S. Taghiyeva, Eur. Phys. J. C **81**, 1080 (2021).
[60] Y. Chen and M. Huang, Phys. Rev. D **105**, 026021 (2022).
[61] E. F. Capossoli, J. P. M. Graça, and H. Boschi-Filho, Phys. Rev. D **105**, 026026 (2022).
[62] P. Colangelo, F. Giannuzzi, S. Nicotri, and V. Tangorra, Eur. Phys. J. C **72**, 2096 (2012).
[63] K. Chelabi, Z. Fang, M. Huang, D. Li, and Y.-L. Wu, J. High Energy Phys. 04 (2016) 036.
[64] D. Li and M. Huang, J. High Energy Phys. 02 (2017) 042.
[65] K. Chelabi, Z. Fang, M. Huang, D. Li, and Y.-L. Wu, Phys. Rev. D **93**, 101901 (2016).

[66] Z. Fang, Y.-L. Wu, and L. Zhang, Phys. Rev. D **99**, 034028 (2019).
[67] D. M. Rodrigues, D. Li, E. Folco Capossoli, and H. Boschi-Filho, Phys. Rev. D **103**, 066022 (2021).
[68] S. P. Bartz and T. Jacobson, Phys. Rev. D **94**, 075022 (2016).
[69] S. P. Bartz and T. Jacobson, Phys. Rev. C **97**, 044908 (2018).
[70] Z. Fang, Y.-L. Wu, and L. Zhang, Phys. Lett. B **762**, 86 (2016).
[71] D. Li, M. Huang, Y. Yang, and P.-H. Yuan, J. High Energy Phys. 02 (2017) 030.
[72] M. Lv, D. Li, and S. He, J. High Energy Phys. 11 (2019) 026.
[73] X. Cao, H. Liu, D. Li, and G. Ou, Chin. Phys. C **44**, 083106 (2020).
[74] J. Chen, S. He, M. Huang, and D. Li, J. High Energy Phys. 01 (2019) 165.
[75] A. Cherman, T. D. Cohen, and E. S. Werbos, Phys. Rev. C **79**, 045203 (2009).
[76] L. Weijian, X. Cao, H. Liu, and D. Li, Pion quasiparticles in isospin medium from holography (to be published).
[77] A. Ali Khan *et al.* (*CP*-PACS Collaboration), Phys. Rev. D **63**, 034502 (2000).
[78] A. Bazavov *et al.* (HotQCD Collaboration), Phys. Rev. D **85**, 054503 (2012).
[79] J. P. Boyd, *Chebyshev and Fourier Spectral Methods* (Dover Publications, Mineola, New York, 2001).
[80] J. S. Hesthaven, S. Gottlieb, and D. Gottlieb, *Spectral Methods for Time-Dependent Problems* (Cambridge University Press, Cambridge, England, 2007), Vol. 21.
[81] M. Suzuki, Phys. Lett. **58A**, 435 (1976).
[82] J. Zinn-Justin, *Quantum Field Theory and Critical Phenomena* (Oxford University Press, Oxford, United Kingdom, 2021), Vol. 171.
[83] M. Flory, S. Grieninger, and S. Morales-Tejera, arXiv:2209.09251.
[84] P. C. Hohenberg and B. I. Halperin, Rev. Mod. Phys. **49**, 435 (1977).
[85] D. T. Son and M. A. Stephanov, Phys. Rev. Lett. **88**, 202302 (2002).
[86] D. T. Son and M. A. Stephanov, Phys. Rev. D **66**, 076011 (2002).
[87] D. T. Son and A. O. Starinets, J. High Energy Phys. 09 (2002) 042.
[88] A. S. Miranda, C. A. Ballon Bayona, H. Boschi-Filho, and N. R. F. Braga, J. High Energy Phys. 09 (2009) 119.
[89] J. Adam *et al.* (STAR Collaboration), Phys. Rev. C **103**, 034908 (2021).
[90] R. Baltensperger and J.-P. Berrut, Comput. Math. Appl. **37**, 41 (1999).